Science of the Total Environment 894 (2023) 164920

Contents lists available at ScienceDirect

Science of the Total Environment

journal homepage: www.elsevier.com/locate/scitotenv

Interpretation of the effects of anthropogenic chlorine on nitrate formation over northeast Asia during KORUS-AQ 2016

Hyun-Young Jo [a], Jaehyeoung Park [b], Gookyoung Heo [c,d], Hyo-Jung Lee [b], Wonbae Jeon [b], Jong-Min Kim [b], Saewung Kim [e], Jung-Kwon Kim [f], Yiming Liu [g], Pengfei Liu [h], Bingqing Zhang [h], Cheol-Hee Kim [a,b,*]

[a] Institute of Environmental Studies, Pusan National University, Busan 46241, Republic of Korea
[b] Department of Atmospheric Sciences, Pusan National University, Busan 46241, Republic of Korea
[c] National Air Emission Inventory and Research Center, Ministry of Environment, Cheongju 28166, Republic of Korea
[d] Now at Environmental Satellite Center, National Institute of Environmental Research, Incheon 22689, Republic of Korea
[e] Department of Earth System Science, University of California, Irvine, Irvine, CA, USA
[f] Department of Environmental Engineering, Dong-Eui University, Busan 47340, Republic of Korea
[g] School of Atmospheric Sciences, Sun Yat-sen University, Zhuhai, China
[h] School of Earth and Atmospheric Sciences, Georgia Institute of Technology, Atlanta, GA 30332, USA

HIGHLIGHTS

- Modeling nitrate formation including Cl emissions in $ClNO_2$ chemistry is crucial in Northeast Asia due to the growing significance of nitrate.
- The WRF-CMAQ model employed the recent Cl emissions and assessed the NO_3^- formation pathways during the KORUS-AQ campaign.
- Despite limited Cl emissions' impact on NO_3^- formation, the simulation showed a reduced 18.7% bias compared to 21.1% without Cl emissions.
- Cl emissions in $ClNO_2$ chemistry may improve $PM_{2.5}$ and inorganic ion predictions, especially in NOx-rich urban areas over Northeast Asia.

GRAPHICAL ABSTRACT

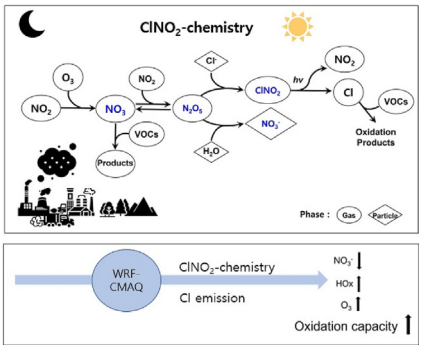

ARTICLE INFO

Editor: Hai Guo

Keywords:
N_2O_5 heterogeneous chemistry
$ClNO_2$ chemistry
Cl emission
Particulate nitrate
CMAQ modeling

ABSTRACT

The Weather Research and Forecasting–Community Multiscale Air Quality (WRF-CMAQ) model, implemented with anthropogenic chlorine (Cl) emissions, was evaluated against ground and NASA DC-8 aircraft measurements during the Korea-United States Air Quality (KORUS-AQ) 2016 campaign. The latest anthropogenic Cl emissions, including gaseous HCl and particulate chloride (pCl^-) emissions from the Anthropogenic Chlorine Emissions Inventory of China (ACEIC-2014) (over China) and a global emissions inventory (Zhang et al., 2022) (over outer China), were used to examine the impacts of Cl emissions and the role of nitryl chloride ($ClNO_2$) chemistry in N_2O_5 heterogeneous reactions on secondary nitrate (NO_3^-) formation across the Korean Peninsula. The model results against aircraft measurements clearly showed significant Cl- underestimations due mainly to the high gas-particle (G/P) partitioning ratios at aircraft measurement altitudes such as 700–850 hPa, but the $ClNO_2$ simulations were reasonable. Several simulations of CMAQ-based sensitivity experiments against ground measurements indicated that although addition of Cl emission did not significantly alter NO_3^- formation, the activated $ClNO_2$ chemistry with Cl emissions showed the best model performance with the reduced normalized mean bias (NMB) of 18.7 % compared to a value of 21.1 %

* Corresponding author at: Department of Atmospheric Sciences, Pusan National University, 30 San, Jangjeon-Dong, Geumjeong-Gu, Busan 609-735, Republic of Korea.
E-mail address: chkim2@pusan.ac.kr (C.-H. Kim).

http://dx.doi.org/10.1016/j.scitotenv.2023.164920
Received 9 March 2023; Received in revised form 13 June 2023; Accepted 13 June 2023
Available online 16 June 2023

for the Cl emissions-free case. In our model evaluation, $ClNO_2$ accumulated during the night but quickly produced Cl• radical due to $ClNO_2$ photolysis at sunrise, which modulated other oxidation radicals (e.g., ozone [O_3] and hydrogen oxide radicals [HO_x]) in the early morning. In the morning hours (0800–1000 LST), the HO_x were the dominant oxidants, contributing 86.6 % of the total oxidation capacity (sum of major oxidants such as O_3 and HO_x species), while oxidability was enhanced by up to ~6.4 % (increase in 1 h HO_x average of 2.89 × 10^6 molecules·cm^{-3}) in the early morning mainly due to the changes in OH (+7.2 %), hydroperoxyl radical (HO_2)(+10.0 %), and O_3 (+4.2 %) over the Seoul Metropolitan Area, during the KORUS-AQ campaign. Our results improve understanding of the atmospheric changes in the $PM_{2.5}$ formation pathway caused by $ClNO_2$ chemistry and Cl emissions over northeast Asia.

1. Introduction

Nitrate (NO_3^-), a component of secondary particulate matter, accounts for a significant proportion of particulate matter <2.5 μm in size ($PM_{2.5}$) in the atmosphere, and is a source of uncertainty in $PM_{2.5}$ operational predictions over northeast Asia (Xiao et al., 2020; Jo et al., 2020; Kim et al., 2021b). NO_3^-, as a major constituent of $PM_{2.5}$, participates in highly complex reactions as a gaseous precursor to secondary particulate matter and is relatively easy to volatilize. It is converted into an aerosol through various chemical pathways including gaseous photochemical and heterogeneous reactions. NO_3^- is formed by the photochemical reactions associated with the hydroxyl radical (OH) and NO_2 in the daytime; however, the nighttime heterogeneous hydrolysis of dinitrogen pentoxide (N_2O_5) plays an important role in nocturnal secondary NO_3^- formation in urban areas. Therefore, to improve NO_3^- prediction accuracy, both daytime and nighttime reactions and their mechanisms need to be clarified when simulating secondary formation of NO_3^-.

Recent ground measurements over northeast Asia have revealed very high NO_3^- concentrations in $PM_{2.5}$ (Jo et al., 2020). Previous studies have reported that 75 % of particulate matter <1.0 μm in size ($PM_{1.0}$) is composed of fine secondary particles formed from gaseous precursors, highlighting the problems presented by fine secondary particles including NO_3^- in South Korea (Shon et al., 2012). In China, more recent data have shown that atmospheric sulfate (SO_4^{2-}) has decreased, while NO_3^- has increased in recent years, which is consistent with the trends of their respective gaseous precursor emissions (Tian et al., 2017; Tian et al., 2019; Wang et al., 2017; Yang et al., 2011). High NO_3^- concentrations were reported during several haze episodes in China (Li et al., 2018; Tian et al., 2017; Yang et al., 2017). Changes in both the amount and chemical properties of $PM_{2.5}$ can be ascribed to the secondary generation of NO_3^-; thus, controlling NO_3^- is important for achieving $PM_{2.5}$ reductions over northeast Asia.

Chlorine (Cl) chemistry and its associated species such as the chlorine radical (Cl•) and nitryl chloride ($ClNO_2$) are involved in the secondary NO_3^- formation pathways, and also have an impact on air quality and oxidation capacity in the atmosphere (Wang et al., 2019; Wang et al., 2020; Zhang et al., 2022). Therefore, to establish national policies to reduce $PM_{2.5}$, it is important to fully understand the contribution of Cl chemistry to secondary NO_3^- formation. In addition, gaseous hydrogen chloride (HCl) and particulate chloride (pCl^-) are also controlling factors in gas–particle (G/P) partitioning processes and aerosol water uptake, enhancing particulate formation during both nighttime and daytime. This is particularly important because Cl^- reacts with N_2O_5 during the nighttime and forms $ClNO_2$, which is the most critical factor in the rapid formation of aerosol NO_3^- at high levels in NO_x-rich environments. During the following daytime, $ClNO_2$ releases Cl^- via photolysis and subsequently oxidizes volatile organic compounds (VOCs), further influencing the formation of daytime ozone (O_3) and particulate matter (Sommariva et al., 2021).

Several atmospheric Cl species have been measured in previous studies, and the importance of $ClNO_2$ chemistry associated with the N_2O_5 reaction has been emphasized over the source areas in northeast Asia. Xiao et al. (2020) reported that 2 min average active Cl_2 and $ClNO_2$ concentrations presented maximum values of 1000 and 1200 pptv, respectively, and the N_2O_5 (2 min average) and NO_3^- (5 min average) concentrations were 40 pptv and 5 μg m^{-3}, respectively. Their study addressed the role of $ClNO_2$ in N_2O_5 heterogeneous chemistry during periods of severe summer air pollution in Beijing (e.g., June 2017). Despite these measurements of $ClNO_2$ chemistry, numerical model studies have struggled to reproduce and interpret the Cl-related chemistry, particularly over northeast Asia and its downwind areas. This has mainly been attributed to the lack of recent Cl emissions that has hindered the quantitative evaluation of the role of $ClNO_2$ chemistry in the process of NO_3^- secondary formation. However, gridded global anthropogenic Cl emissions inventories have been developed based on published up-to-date activity data and emissions factors (Sarwar et al., 2012; Zhang et al., 2022), and chemical transport models have been increasingly used to interpret the effects of $ClNO_2$ on N_2O_5 heterogeneous chemistry. Sarwar et al. (2012) investigated the effects of $ClNO_2$ production and Cl species activation by implementing the heterogeneous synthesis of $ClNO_2$ based on the parametrization of uptake processes and additional gaseous Cl_2 reactions in the Community Multiscale Air Quality (CMAQ) model that were also previously proposed by Bertram and Thornton (2009). They showed that $ClNO_2$ production reduced the total NO_3^- levels in the United States (by up to 0.8–2.0 μg m^{-3} or 11–21 %) and had a minor impact on 8 h O_3 levels (by up to 1–2 ppb or 3–4 %). Later, Sarwar et al. (2014) applied the model to the entire Northern Hemisphere and found that $ClNO_2$ production had a significant impact on increasing 8 h O_3 levels to 7.0 ppb, with a particularly high impact over China and Western Europe.

Northeast Asia is a well-known transboundary pollution region (Park et al., 2005; Kim et al., 2012; Kim et al., 2018; Lee et al., 2019; Jo et al., 2020; Kim et al., 2021a, 2021b; Lee et al., 2021; Lee et al., 2022), in which anthropogenic aerosols and their precursors emitted from upwind areas can be subjected to long-range transport (LRT) to downwind areas. Therefore, studies of $ClNO_2$ chemistry and its impact on the neighboring countries in northeast Asia are also becoming important in cases where NO_3^- is a major factor in high $PM_{2.5}$ episodes. However, it is difficult to interpret the LRT process in NO_3^- formation in association with the $ClNO_2$-chemistrty over the downwind areas, mainly due to the lack of measurements of Cl species such as Cl_2 and $ClNO_2$ over the downwind areas in northeast Asia. Recently, a ground and aircraft measurement of multiple chemical components of the atmosphere, including Cl species, was carried out over the Korean Peninsula through the 2016 Korea-United States Air Quality Study (KORUS-AQ). The campaign was jointly hosted by the Korean National Institute of Environmental Research (NIER) and NASA during May–June 2016 (Lee et al., 2020; Crawford et al., 2021; Kim et al., 2021a, 2021b; Park et al., 2021), and determined the concentrations of Cl species over the Seoul Metropolitan Area (SMA).

Comprehensive modeling studies of NO_3^- formation considering Cl emissions over northeast Asia, including its downstream areas such as Korean Peninsula, are scarce because of the lack of Cl emissions data covering the domain and the limited measurements of Cl species such as $ClNO_2$ and Cl_2. In China, several regional air quality models with updated $ClNO_2$ chemistry (i.e., CMAQ) have been developed using the Anthropogenic Chlorine Emissions Inventory of China (ACEIC) 2014. Studies of $ClNO_2$ chemistry are also being conducted to determine its impact on NO_3^- and O_3 concentrations. In addition, for a Cl emissions assessment over northeast Asia, KORUS-AQ measurements (Jeong et al., 2019) can be used to evaluate the role of $ClNO_2$ chemistry and heterogeneous uptake processes in a more quantitative manner and to interpret the $ClNO_2$ chemical reactions in the process of secondary NO_3^- formation over the downwind areas in northeast Asia.

In this study, we used the most recent anthropogenic Cl emissions inventory over the entire region in northeast Asia, and carried out Weather Research and Forecasting–CMAQ (WRF-CMAQ) simulations for the period covering the KORUS-AQ campaign. The improved $ClNO_2$ heterogeneous chemistry implemented in CMAQ (ver. 5.3.2) was employed and several sensitivity tests were conducted to investigate the effect of nighttime $ClNO_2$ processes on the uptake coefficient of N_2O_5 and NO_3^- production. In addition to the integrated effects caused by the $ClNO_2$ resulting from Cl emissions on the atmospheric chemical properties of $PM_{2.5}$, the changes in atmospheric oxidation capacity (i.e., O_3 and hydrogen oxide radicals [HO_x]) were also investigated. We considered the full heterogeneous $ClNO_2$ chemistry and Cl emissions over the entire northeast Asia. It was anticipated that the results would enable rational $PM_{2.5}$ reduction strategies to be established in a more scientific way, particularly in the NO_x-rich urban areas over northeast Asia.

2. Methods and data

2.1. Role of $ClNO_2$ in N_2O_5 heterogeneous chemistry

Particulate NO_3^- can be formed via multiple pathways, including daytime photochemical processes and nighttime NO_3^- formation. NO_x is primarily removed from the atmosphere during the daytime through the formation of HNO_3, which is created by the reaction of NO_2 and OH. During the nighttime, however, N_2O_5 is an important reactive species in the polluted atmosphere, and its uptake process is the dominant pathway in the formation of particulate NO_3^-. During the formation of particulate NO_3^-, an important aspect of the N_2O_5 heterogeneous chemistry is its reaction with Cl^- to produce $ClNO_2$. $ClNO_2$ is stable at night but is completely photolyzed approximately 1 h after sunrise the next morning. In the presence of chloride particles, the heterogeneous hydrolysis of N_2O_5 can produce either $ClNO_2$ or nitric acid (HNO_3), whereas the heterogeneous hydrolysis of N_2O_5 produces only HNO_3 in the absence of chloride particles. The main Cl chemical reactions associated with the formation of particulate NO_3^-, can be summarized as the following ten reactions.

$$NO_{2(g)} + O_{3(g)} \rightarrow NO_{3(g)} + O_{2(g)} \quad \text{(R1)}$$

$$NO_{3(g)} + NO_{2(g)} \rightarrow N_2O_{5(g)} \quad \text{(R2)}$$

$$N_2O_{5(g)} \rightarrow NO_{3(g)} + NO_{2(g)} \quad \text{(R3)}$$

$$N_2O_{5(g)} + H_2O_{(het)} \rightarrow 2HNO_{3(aq)} \quad \text{(R4)}$$

$$N_2O_{5(g)} + (1 - Y)\, H_2O_{(het)} + Y \cdot HCl_{(aq)} \rightarrow Y \cdot ClNO_{2(g)} + (2 - Y) \cdot HNO_{3(aq)} \quad \text{(R5)}$$

$$ClNO_{2(g)} + hv \rightarrow Cl_{(g)} + NO_{2(g)} \quad \text{(R6)}$$

$$Cl_{(g)} + O_{3(g)} \rightarrow ClO_{(g)} + O_{2(g)} \quad \text{(R7)}$$

$$ClO_{(g)} + NO_{2(g)} \rightarrow ClONO_{2(g)} \quad \text{(R8)}$$

$$ClONO_{2(g)} + H_2O_{(g)} \rightarrow HOCl_{(g)} + HNO_{3(aq)} \quad \text{(R9)}$$

$$ClONO_{2(g)} + H_2O_{(g)} \rightarrow Cl_{2(g)} + HNO_{3(aq)} \quad \text{(R10)}$$

The reactions (R1)–(R5) summarize the NO_3^- formation mechanism via N_2O_5 uptake processes and $ClNO_2$ production. The heterogeneous absorption of N_2O_5 produces HNO_3 on the surface of an aerosol containing water through reaction (R4), and also produces HNO_3 and gaseous $ClNO_2$ on the surface of an aerosol containing chloride through reaction (R5) (Finlayson-Pitts et al., 1989; Osthoff et al., 2008). In (R5), parameter Y denoted the $ClNO_2$ yield, representing the fraction of N_2O_5 that reacts via reaction (R5) instead of reaction (R4), and is calculated by the following equation (Bertram and Thornton, 2009).

$$Y = \left(1 + \frac{[H_2O]}{483 \times [Cl^-]}\right)^{-1} \quad (1)$$

It should be noted that the reactions (R1) and (R5) has an impact on the nitrate radical (NO_3), which in turn reacts with a number of volatile organic compounds (VOCs) such as isoprene, monoterpenes, and phenols and contributes to formation of peroxy (or hydroxyl) radicals, organic nitrates, and HNO_3. The $ClNO_2$ generated can be photolyzed into Cl• and nitrogen dioxide (NO_2) through reaction (R6). A series of reactions (R7)–(R10) also leads to total nitrate reactions (Platt et al., 1990; Atkinson, 2000; Monks, 2005). A schematic illustration of heterogeneous $ClNO_2$ chemistry in association with HNO_3 generation is shown in Fig. 1.

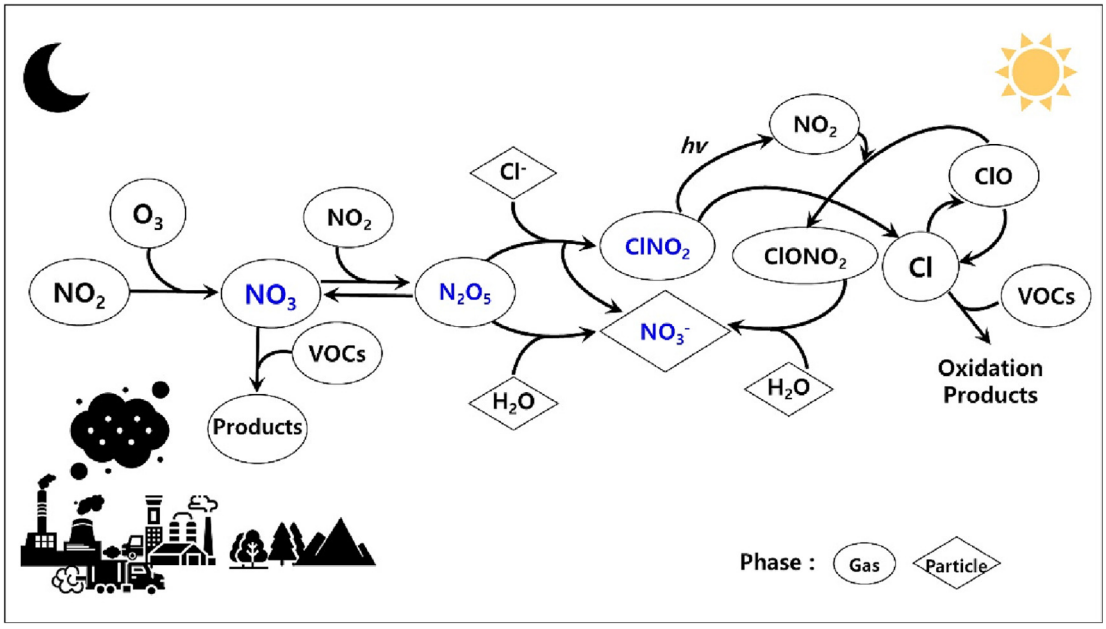

Fig. 1. Schematic illustration of $ClNO_2$ chemistry during the secondary NO_3^- formation process.

2.2. Numerical modeling system and domain

The CMAQ model (ver. 5.3.2) (https://www.epa.gov/cmaq) was used for the regional air quality simulations. It contains a carbon bond chemistry mechanism with halogen chemistry (Appel et al., 2017). For the meteorological input field for the CMAQ simulation, the WRF model (ver. 4.1.1) was used. The meteorological/chemical/physical parameters used in previous modeling studies are listed in Table S1. The major uncertainties in these modeling studies were the nighttime N_2O_5 uptake coefficients and $ClNO_2$ production process; we adopted the parametrization of a heterogeneous N_2O_5 uptake process (Jo et al., 2019, 2022), and $ClNO_2$ production as proposed by Bertram and Thornton (2009), which have been used in previous studies.

The horizontal domain for the WRF-CMAQ simulations included two nested domains with horizontal resolutions of 27 and 9 km over the SMA, as shown in Fig. 2. Domain 1 (D1) included East Asia, with a 27 km grid resolution (178 × 142), and Domain 2 (D2) included eastern China, the Yellow Sea, and South Korea (Fig. 1), with a 9 km grid resolution (166 × 199). For the vertical resolution, 35 layers were considered with the top layer set to 100 hPa. For the meteorological simulation by WRF, the initial and boundary data were 0.25° × 0.25° Final Operation Global Analysis (FNL) data (ds083.3) from the National Centers for Environmental Prediction (NCEP), and the numerical simulation covered the period between 0900 LST, April 30, 2016, and 0900 LST, June 14, 2016, which was the KORUS-AQ campaign period. The detailed settings applied in the meteorology and air quality modeling are presented in Table S1.

2.3. Emissions data

Most modeling studies have used gaseous HCl and particulate Cl^- (pCl^-) emissions as the anthropogenic Cl emissions, and then attempted to interpret the role of $ClNO_2$ and N_2O_5 in global- or regional chemical transport models. However, Cl emissions are a fundamental input in air quality models to simulate NO_3^- formation, but they are subject to uncertainty and errors. The Reactive Chlorine Emissions Inventory (RCEI) (Keene et al., 1999), which represents global anthropogenic Cl emissions, has been used in previous studies of the Cl emissions used in models. It was compiled in 1990, but it has a poor spatial resolution and a higher bias compared to current observations and/or recent local Cl emissions estimates. Consequently, it was expected that there may be substantial uncertainties in the retransmission of emissions. Anthropogenic Cl emissions over northeast Asia have not been included in most previous simulations although they are crucial for simulating N_2O_5 uptake and the activation of Cl chemistry.

Recently, the ACEIC 2014 anthropogenic Cl emissions (HCl and pCl^-) inventory (Liu et al., 2018; Hong et al., 2020a, 2020b; Zhang et al., 2022), and a global emissions inventory (Zhang et al., 2022) have been developed. We used the combined Cl emissions from ACEIC 2014 for inland China, and the global emissions for the region outside of China including the Korean Peninsula. The ACEIC (2014) was developed for China with a horizontal resolution of 0.1° × 0.1° and has been used in previous modeling studies. The sectoral Cl emissions in ACEIC were reported to be 254, 253, 251, 109, and 65 Gg Cl from agricultural fuels, residential biofuels, waste incineration, coal combustion, and industrial processes, respectively. The details were reported in previous studies (Liu et al., 2018; Hong et al., 2020a, 2020b; Zhang et al., 2022). Emissions over the outside domain of China were extracted from a global emissions inventory, which was developed using published up-to-date activity data and emissions factors based on 35 sources categorized into six source sectors (Zhang et al., 2022). The ACEIC emissions sources we used for inland China were anthropogenic, whereas the global emissions that applied to the region outside of China consisted of anthropogenic sources. The spatial distributions of the merged ACEIC emissions with global Cl emissions (HCl and pCl^-) with a resolution of 0.1° × 0.1° for 2014 are shown in Fig. S1.

For the emissions of other inorganic and organic species needed in the CMAQ model in the current study, we used the Mosaic Asian Anthropogenic Emissions Inventory (MIX) 2010 (Li et al., 2017; Souri et al., 2017) for the entire domain of the Asia region, and the Clean Air Policy Support System (CAPSS) 2016 for South Korea. The Model of Emissions of Gases and Aerosols from Nature (MEGAN) version 2.04 was used for biogenic emissions.

2.4. KORUS-AQ field campaign and DC-8 aircraft measurements

The KORUS-AQ campaign was jointly conducted by NIER and NASA during the period of May 1–June 12, 2016. Details of the KORUS-AQ campaign are provided by Crawford et al. (2021). During the campaign, comprehensive measurements of trace gases and aerosol particle properties were collected from DC-8 aircraft, ground sites, and ships with a broad spatial and verification coverage. The Cl species were measured from both

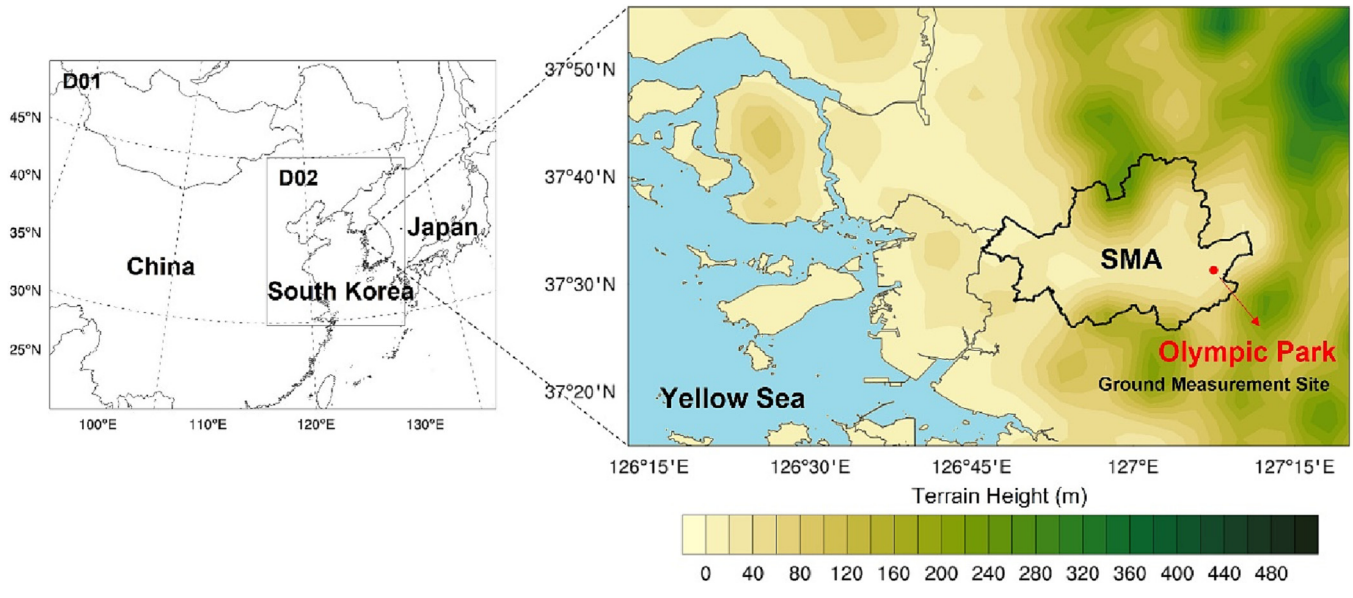

Fig. 2. Modeling domains (27 and 9 km grid resolution) and terrain features over the Seoul Metropolitan Area (SMA). The red dot represents the ground measurement (Olympic Park; OP) site in the SMA.

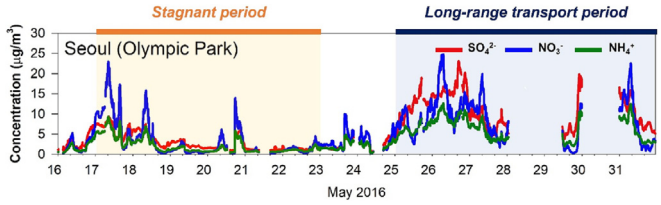

Fig. 3. Temporal variation in NO_3^-, SO_4^{2-}, and NH_4^+ concentrations measured at the OP site for May 2016, including the stagnant (STG) and long-range transport (LRT) periods. The STG and LRT cases were classified by Peterson et al. (2019).

aircraft and ground site measurements. The pathways and flight altitudes of the DC-8 air flights have previously been reported (Crawford et al., 2021; Kim et al., 2021a, 2021b), and the location of the ground measurement site (Olympic Park: OP) in southeast Seoul is indicated in Fig. 2.

Measurements of Cl species such as $ClNO_2$ and Cl_2 were compared to the results from the WRF-CMAQ modeling. During the KORUS-AQ campaign, the $ClNO_2$ and Cl_2 were simultaneously measured via chemical ionization mass spectrometry (THS Instruments Inc., Atlanta, GA, USA), and the molecules of interest were ionized into ion clusters prior to their detection with a quadrupole mass spectrometer. Together with the Cl species, the relevant trace gas and aerosol components were also measured during the KORUS-AQ campaign. The settings, precision, and accuracy of all instruments used during the campaign were previously described (Jeong et al., 2019).

The weather conditions during the KORUS-AQ campaign exhibited various air pollution characteristics. In Peterson et al. (2019), the weather conditions during a full month of the campaign were classified into four periods: dynamic meteorology (May 4–16), stagnant (May 7–22), transport (May 25–31), and blocking pattern (June 1–7) periods. We focused on the second half of the KORUS-AQ campaign, because $PM_{2.5}$ concentrations were generally low in the first half, whereas there were two peak periods: stagnant (STG; May 17–22) and long-range transport (LRT; May 25–31). Both cases had high pollutant concentrations under the contrasting meteorological conditions, and the potential contribution of transboundary $ClNO_2$ to NO_3^- production could be better diagnosed by contrasting the two periods.

Fig. 3 shows the hourly variation in $PM_{2.5}$, SO_4^{2-}, NO_3^-, and ammonium (NH_4^+) concentrations measured at the OP site (Fig. 2) for the period of May 16–31, 2016. The overall measurements indicated that NO_3^- concentrations rapidly increased during the STG period (May 17–22), and it was believed that heterogeneous N_2O_5 uptake and $ClNO_2$ production reactions would also be associated. In comparison, higher NO_3^- and SO_4^{2-} concentrations were also measured during the LRT period (May 25–31).

3. Design of sensitivity simulations for interpreting Cl emissions and $ClNO_2$ chemistry

In this study, several numerical WRF-CMAQ sensitivity simulations were designed to investigate the relationship between N_2O_5 uptake and $ClNO_2$ production during the study period. The framework of the sensitivity experiments included the "base case" that was commonly employed in previous studies. Further simulations were tested by activating the $ClNO_2$ chemistry and/or loading (or unloading) the Cl (pCl^- and HCl) emissions, and then examining the differences between the simulations.

Table 1 summarizes the four sensitivity experiments designed in this study. We first conducted Exp1 as the base case. Where only a heterogeneous N_2O_5 uptake process (without $ClNO_2$ chemistry) was employed, as previously adopted by Jo et al. (2019, 2022). Therefore, Exp1 (base case) only accounted for nighttime HNO_3 generation by considering the heterogeneous absorption of N_2O_5 on the aerosol surface, where HNO_3 was produced by the heterogeneous hydrolysis of N_2O_5. Exp2 (denoted as HET_n + Cl_n) was designed to examine the effect of disregarding both N_2O_5 uptake and $ClNO_2$ chemistry; thus, all of the chemical processes relevant to both N_2O_5 and $ClNO_2$ heterogeneous chemistry were disregarded. The other experiments (Exp3 and Exp4) sequentially evaluated the effects of heterogeneous $ClNO_2$ chemistry on NO_3^- formation by comparing against the base case. Exp3 (denoted as HET + Clm_n) was the base case plus $ClNO_2$ chemistry, but without loading the Cl emissions (thus HCl and pCl^- were off) to evaluate the sole contribution of $ClNO_2$ chemistry to the NO_3^- formation without Cl emissions. Exp4 (denoted as HET + Cl) was designed to consider the possible N_2O_5 heterogeneous chemistry plus the effects of $ClNO_2$ with anthropogenic Cl emissions loaded. Exp4 was therefore the most detailed experiment in this study and implemented $ClNO_2$ chemistry, while allowing the heterogeneous absorption processes of N_2O_5 on the aerosol surface to produce $ClNO_2$ and HNO_3, with both HCl and pCl^- emissions fully loaded.

4. Results and discussion

4.1. Model evaluation against ground and aircraft measurements

To statistically evaluate the WRF-CMAQ model simulations against ground measurements, we first employed evaluation indices: the normalized mean bias (NMB), index of agreement (IOA), and correlation coefficient (R). Table S2 provides a statistical summary of the four experiments (Exp1 to Exp4) against ground measurements (OP site) for several species, including Cl species such as $ClNO_2$ and Cl^- for the period of May 16–31, 2016.

Although the model performance was not statistically significant (Table S2), Exp4 yielded the best model performance for both $PM_{2.5}$ and inorganic ion components. The evaluation statistics for Exp4 had average values of NMB ± 30 %, IOA 0.62–0.91, and R 0.53–0.85, which were all within the tolerance intervals (NMB ± 30 %, IOA 0.5, and R 0.4 or higher) suggested in previous studies (Emery et al., 2016, Willmott et al., 1985; Hurley et al., 2001). It was also encouraging that the Cl^- in Exp4 correlated well with the measurements, with a reduced NMB (43.15 %) and NME (133.05 %), and better results compared to the average values of NMB (34 ± 95 %) and NME (144 ± 54 %) from the other three experiments.

The simulation results were also compared to the NASA DC-8 aircraft measurements. All flight observation data, such as flight pathways, flight dates, and measurement instruments during the KORUS-AQ campaign have previously been reported (Lee et al., 2020; Crawford et al., 2021;

Table 1
Simulation scenarios for the WRF-CMAQ model used in this study.

Experiment	Name	Chemistry of N_2O_5 and $ClNO_2$ production	Cl emissions
Exp1	Base Case	N_2O_5 heterogeneous uptake process (on) $ClNO_2$ production chemistry (off)	Not considered
Exp2	HET_n + Cl_n	N_2O_5 heterogeneous uptake process (off) $ClNO_2$ production chemistry (off)	Not considered
Exp3	HET + Clm_n	N_2O_5 heterogeneous uptake process (on) $ClNO_2$ production chemistry (on) Gas-phase HCl emissions loaded (off) Particulate Cl^- emissions loaded (off)	Not considered
Exp4	HET + Cl	N_2O_5 heterogeneous uptake process (on) $ClNO_2$ production chemistry (on) Gas-phase HCl emissions loaded (on) Particulate Cl^- emissions loaded (on)	Considered

Kim et al., 2021a, 2021b; Kim et al., 2018). For comparisons of aircraft measurements against WRF-CMAQ model results, we used quantile-quantile (q-q) plots, which are a type of scatterplot wherein the DC-8 flight measurements and WRF-CMAQ simulations were independently sorted. The q-q plots could be used to determine whether the distributions of measured and simulated values were comparable in an aggregated manner, particularly in cases where the WRF-CMAQ model captured extreme flight measurements.

Fig. 4 shows q-q plots for the selected inorganic species (NO_3^-, NH_4^+, Cl^-, and $ClNO_2$) for the period of May 16–31, 2016. As shown in Fig. 4, all of the NO_3^- and NH_4^+ simulations were approximately two-fold underestimated, whereas $ClNO_2$ simulations were within a reasonable range, except for the higher observations (i.e., >400 pptv) in which the model tended to underestimate $ClNO_2$. It should be noted that there was a very poor performance (extreme underestimation) for Cl^- but $ClNO_2$ simulations were acceptable in the non-surface atmosphere over northeast Asia when Cl chemistry was employed (Bertram and Thornton, 2009), which was the approach used in previous studies. In our model analysis, we confirmed that this underestimation arose from the results of the aerosol thermodynamics module ISORROPIA II used in the CMAQ model, in which there was a high gas to particle (G/P) partitioning ratio in simulating aerosol Cl^-. There was a G/P of 0.9 or more at high altitudes such as at DC-8 aircraft measurement altitudes of up to 700–850 hPa, where dry conditions with a relative humidity lower than 40 % imposed considerable limitations on G/P partitioning, as reported in previous thermodynamic studies (Chang et al., 2016; Guo et al., 2016). This suggests that a better understanding of $ClNO_2$ chemistry with a more detailed thermodynamic module would be required for consistent Cl-species simulations in the dry and non-surface atmosphere. It was also noticeable that the higher levels of NO_3^- (and $PM_{2.5}$) resulted in larger biases in Exp2 than in the other three experiments. In Exp4, which was designed to examine the role of Cl emissions against Exp3, a quantifiable difference was found in the amount of simulated $ClNO_2$, indicating that the results of both Exp3 and Exp4 were closer to the aircraft measurements, but Exp4 outperformed Exp3 with a small improvement observed in our study.

4.2. Evaluation of simulated temporal variation in $ClNO_2$ chemistry

Fig. 5 shows the temporal variation in the $PM_{2.5}$ and its inorganic components (NO_3^-, SO_4^{2-}, NH_4^+, and Cl^-) simulated by the four experiments (Exp1 to Exp4) against the ground measurements at the OP site during the campaign (Fig. 2). Daily variation in $PM_{2.5}$ and inorganic ions were well captured during both the STG and LRT periods, with higher $PM_{2.5}$ concentrations measured (and simulated) during the LRT than STG. This was associated with the high fraction of SO_4^{2-} in $PM_{2.5}$ (Fig. 5), which was also discussed by Jo et al. (2020). Of the four experiments, Exp2 had much lower concentrations of all species than the other three experiments, particularly on days with high $PM_{2.5}$ concentrations such as May 17 and May 26, 2016 (Fig. 2). This was undoubtedly because Exp2 did not account for both the heterogeneous uptake of N_2O_5 and $ClNO_2$ chemistry.

In Exp3 (HET + CLm_n) and Exp4 (HET + Cl), which only differed in their Cl emissions loading, the differences in $PM_{2.5}$, NO_3^-, and NH_4^+ concentrations were considerable against Exp1 (base case) particularly for the highest $PM_{2.5}$ episodes. The simulated concentrations in Exp4 were slightly lower than those in Exp3 but were closer to the measurements. This implied that the cases with all Cl emissions (HCL and pCl^-) loaded had a better (but not good) simulation capability for the formation of both NO_3^- and other inorganic species. By contrast, there were substantial differences in Cl^- and

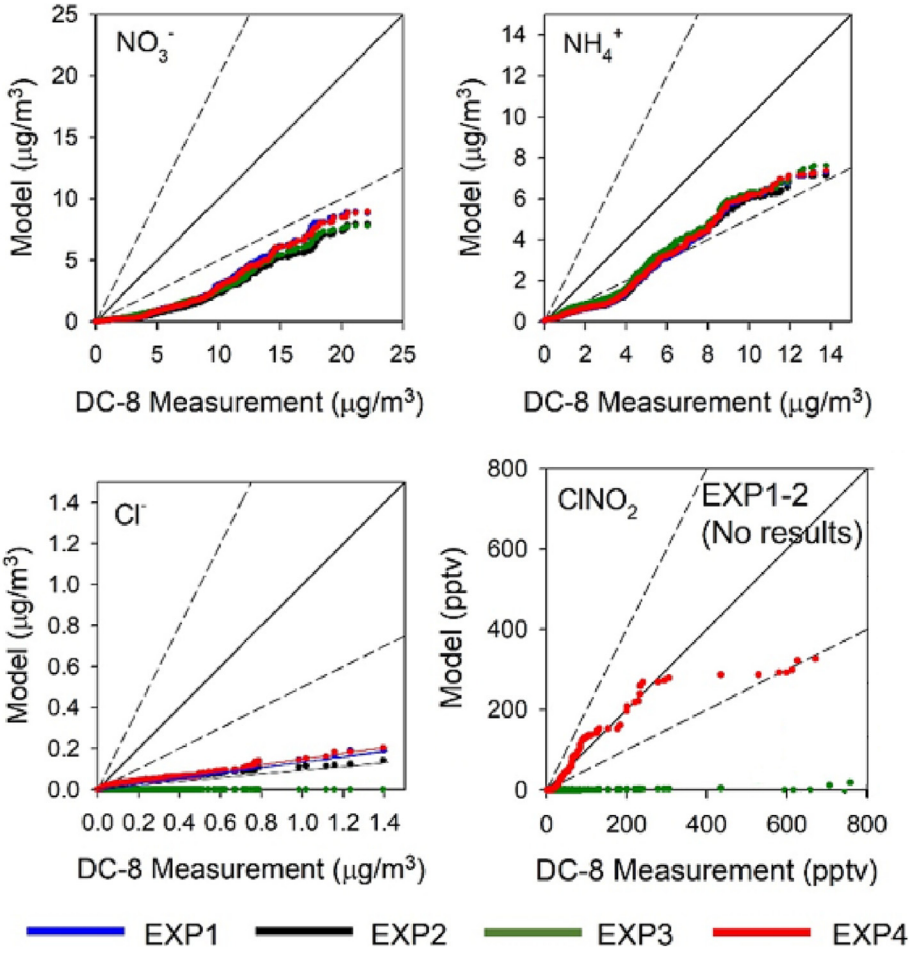

Fig. 4. Quantile-quantile plots for KORUS-AQ DC-8 aircraft PM_1 measurements vs. WRF-CMAQ results for NO_3^-, NH_4^+, Cl^-, and $ClNO_2$ during the KORUS-AQ campaign.

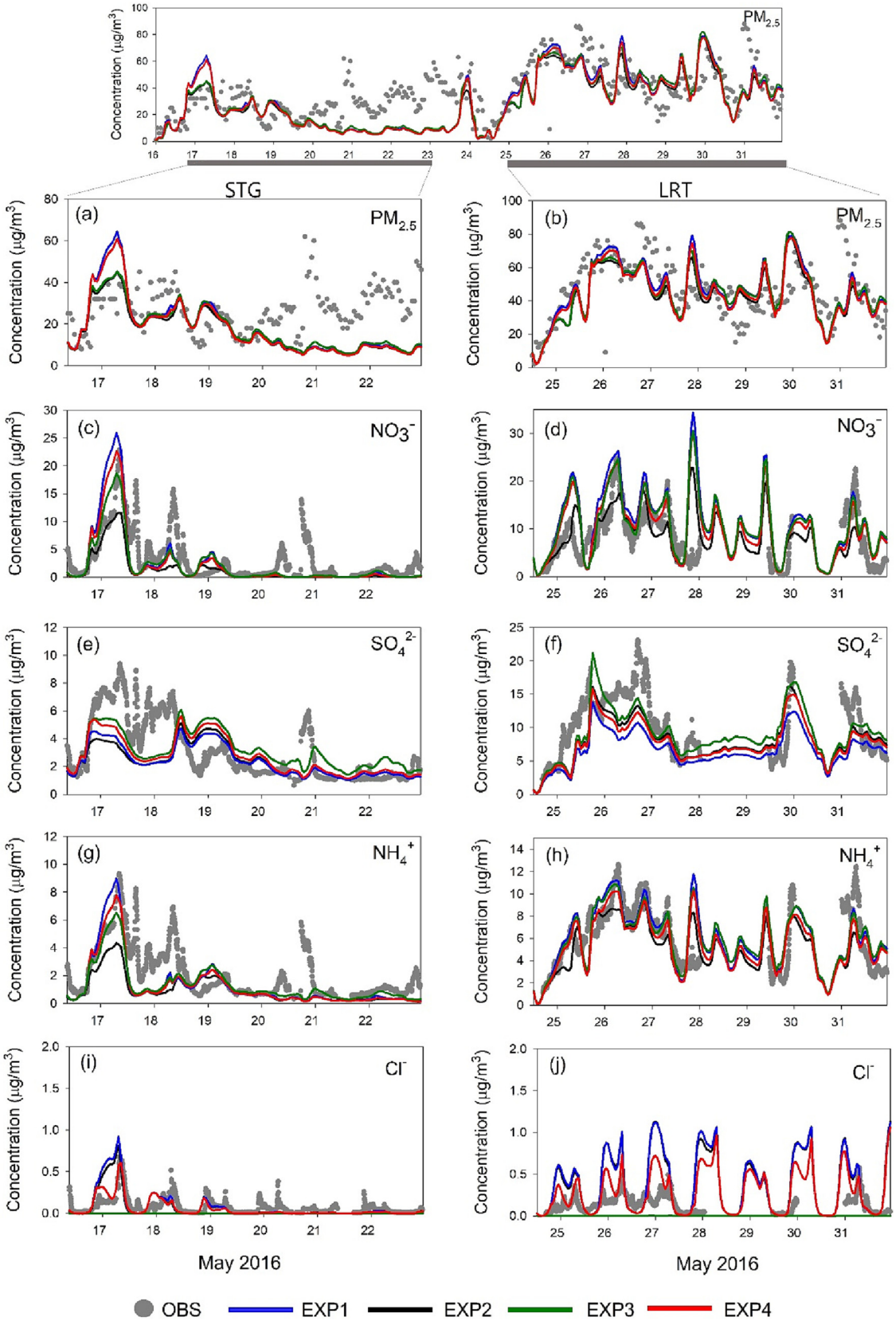

Fig. 5. Comparisons of the time series of measurements (at the OP site) for $PM_{2.5}$, NO_3^-, SO_4^{2-}, NH_4^+, and Cl^- against the simulations from Exp1 to Exp4 for the stagnant (STG) and long-range transport (LRT) periods during KORUS-AQ.

$ClNO_2$ between Exp3 and Exp4, yielding results that were significantly closer to the measurements for Exp4 than those of Exp3. This suggests that the joint consideration of both $ClNO_2$ chemistry and Cl emissions was the best approach to understand the temporal variation in Cl^- and $ClNO_2$ species in $ClNO_2$ chemistry and the subsequent effects on secondary NO_3^- formation processes.

The other inorganic gas-phase species that were simulated, such as O_3 and NO_2, were also compared to ground measurements (Fig. S2). Although there were large differences in the Cl^- concentration between experiments (Figs. 4 and 5), mainly because Exp1 and Exp2 did not account for Cl chemistry, there were only small (almost undetectable) differences in gas species (e.g., O_3 and NO_2 in Fig. S2) between all four experiments. This was even the case in Exp2 where all reactions involved in the N_2O_5 and $ClNO_2$ chemistry were neglected. Only nighttime NO_2 and daytime O_3 showed detectable inter-experimental differences, which was consistent with previous studies of the effects of nighttime $ClNO_2$, and Cl· produced in photochemical reactions (Wang et al., 2020; Zhang et al., 2022). It was therefore interpreted that $ClNO_2$-NO_2 interactions mainly involved nighttime NO_3^- formation but did not significantly alter the gas phase chemicals. However, the $ClNO_2$ was photo-dissociated in the early morning and subsequently produced Cl·, which may have influenced the photochemical reactions leading to O_3 formation. This is discussed in more detail in the next section.

4.3. Integrated Reaction Rates (IRRs) analysis of Cl-chemistry

The formation of HNO_3 is affected by Cl-chemistry through various pathways. Firstly, Cl-chemistry diverts N_2O_5 from forming HNO_3 in thermodynamic equilibrium with NO_3^- to producing $ClNO_2$, and reduces NO_3^-, as seen in reactions (R4)–(R6). Modeling studies have reported several results on N_2O_5 uptake coefficient parameterizations in relation to this process. Bertram and Thornton (2009) reported that considering Cl-chemistry increases the N_2O_5 uptake coefficient, which enhances the formation of nitrate aerosol. However, the increased N_2O_5 uptake coefficient also reduces the abundance of NO_3 radical through reactions (R4)–(R5) during nighttime. Additionally, a series of reactions (R6)–(R10) leads to an increase in HNO_3 production reactions. In this study, we utilized the integrated reaction rates (IRRs) to evaluate the simulated chemical sources and losses of HNO_3 for the Exp4 (HET + Cl). The IRR analysis is a method in the CMAQ model that tracks the chemical reactions' contributions to specific pollutant concentrations.

Fig. 6 displays the results of the IRR analysis from Exp4 for HNO_3 during both daytime and nighttime. As shown in the figure, the dominant source of HNO_3 during the daytime is the reaction of NO_2 + OH, accounting for 98.8 % of all nitrate production with an hourly maximum production rate of 1.69 ppb per hour. During the nighttime, N_2O_5 heterogeneous reactions are the main drivers of HNO_3 production, accounting for approximately 0.2 ± 0.13 ppb per hour (85.4 ± 3.0 %) for the entire study period, with 0.08 ± 0.04 ppb per hour (68.7 ± 29.6 %) for the STG period and 0.31 ± 0.02 ppb per hour (76.1 ± 28.3 %) for the LRT period in this study (Fig. 6). Furthermore, the sequential reactions of (R6)–(R10) have a

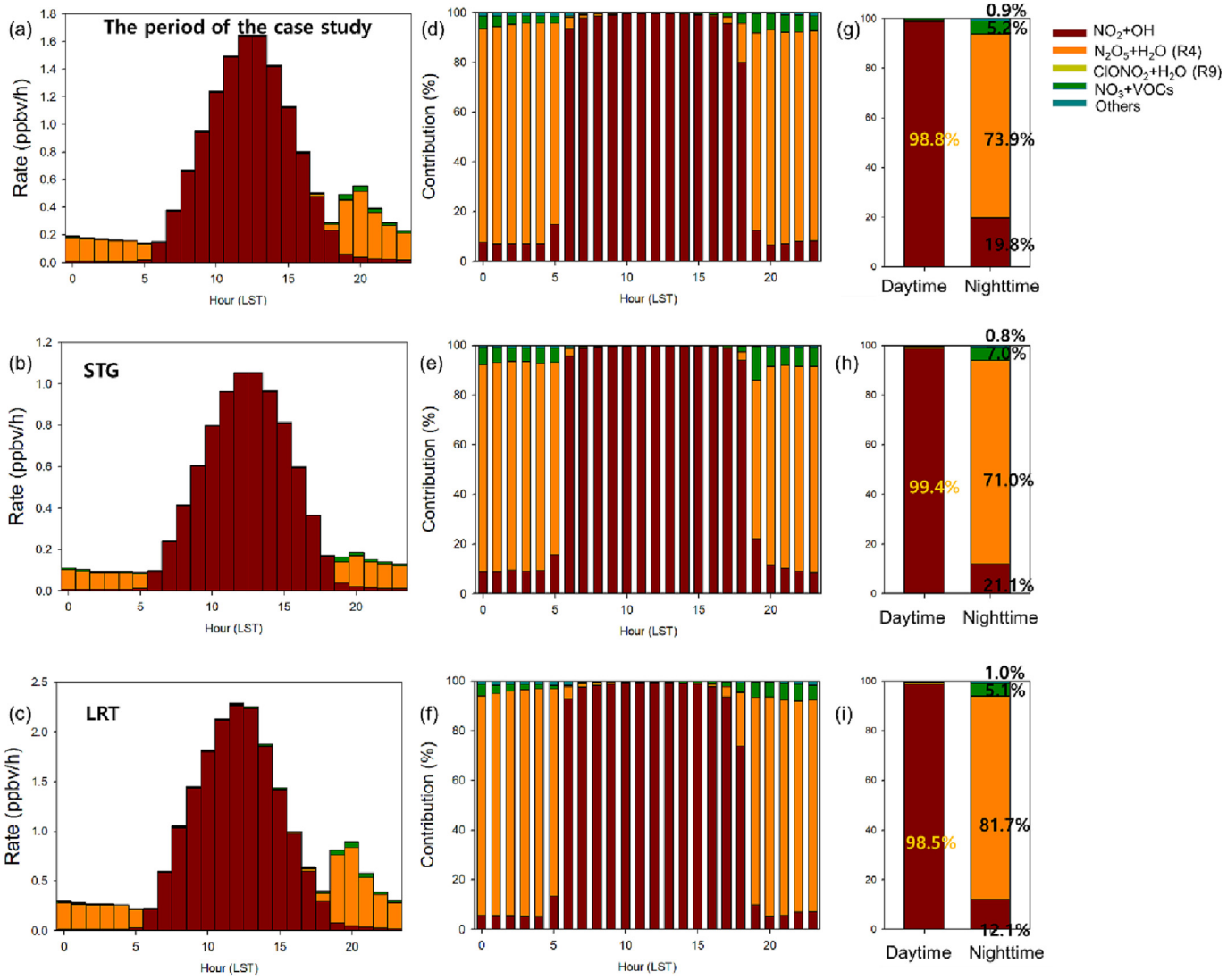

Fig. 6. Diurnal variations of HNO_3 production rates (ppbv per hour) in various different chemical pathways (a–c), and fractional contributions (%) of chemical processes to HNO_3 chemical productions (d–f) at the OP site for Exp4. Also shown are averages of contributions during daytime and nighttime periods (g–i). The top panel presents the results for the entire Korus-AQ campaign period, and the middle and bottom panels show for the STG and LRT cases, respectively.

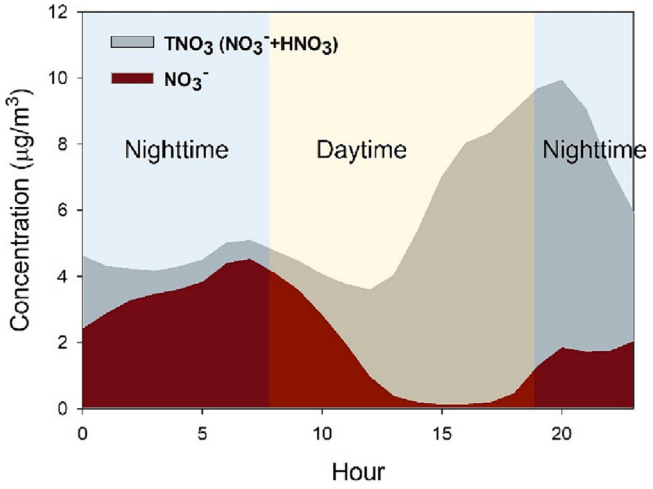

Fig. 7. Simulated temporal variations of total-NO_3 (TNO_3 = particulate NO_3^- + gaseous HNO_3) and particulate NO_3^- (in Exp4) in surface air around the Korean Peninsula.

small but detectable effect of approximately 0.001 ppb per hour (0.1 ± 0.1 %) on the formation of nighttime HNO_3 for the entire study period (Fig. 6). This can be indicating again that HNO_3 was produced by NO_2 + OH through the photochemical oxidation of NO_x during the day, and by the N_2O_5 + H_2O process at night, as estimated by the IRR analysis of the gas-phase chemistry module. The homogeneous formation of HNO_3 from $N_2O_{5(g)}$ + $H_2O_{(g)}$ is a part of the nitrate formation reaction at night, but this homogeneous gas phase reaction proceeds more slowly than the heterogeneous formation of HNO_3 via the heterogeneous hydrolysis of N_2O_5 on or within aqueous aerosol particles.

Considering that the production of HNO_3 (Fig. 6) does not exclusively lead to the formation of particulate nitrate, we conducted further analysis on the partitioning ratios of HNO_3 between the gas and particulate phases. Fig. 7 illustrates the temporal variation of total-NO_3 (TNO_3 = gaseous HNO_3 + particulate NO_3^-) for Exp4 (HET + Cl). From Fig. 7, it is apparent that the daytime OH + NO_2 reaction generates HNO_3, which then undergoes gas-particulate partitioning, resulting in the formation of particulate NO_3^- with G/P partitioning ratios (PR $= \frac{NO_3^-}{TNO_3}$) below 0.5, ranging from 0.01 to 0.5 (Fig. 7). This indicates a tendency for TNO_3 to predominantly exist in the gaseous state. However, during nighttime, direct N_2O_5 hydrolysis produces particulate NO_3^- with a maximum G/P partitioning ratio of 0.9 around 0600LST. This suggests that it is more likely to be present in the form of particulate NO_3^-. These findings highlight the primary contribution of the OH + NO_2 pathway to TNO_3 production in the gaseous state during the day, while the heterogeneous N_2O_5 pathway dominates the production of particulate NO_3^-, making it more prevalent in the particulate state at night.

We also conducted the same Exp4 experiment with halved N_2O_5 uptake coefficient proposed by Bertram and Thornton (2009) to examine the

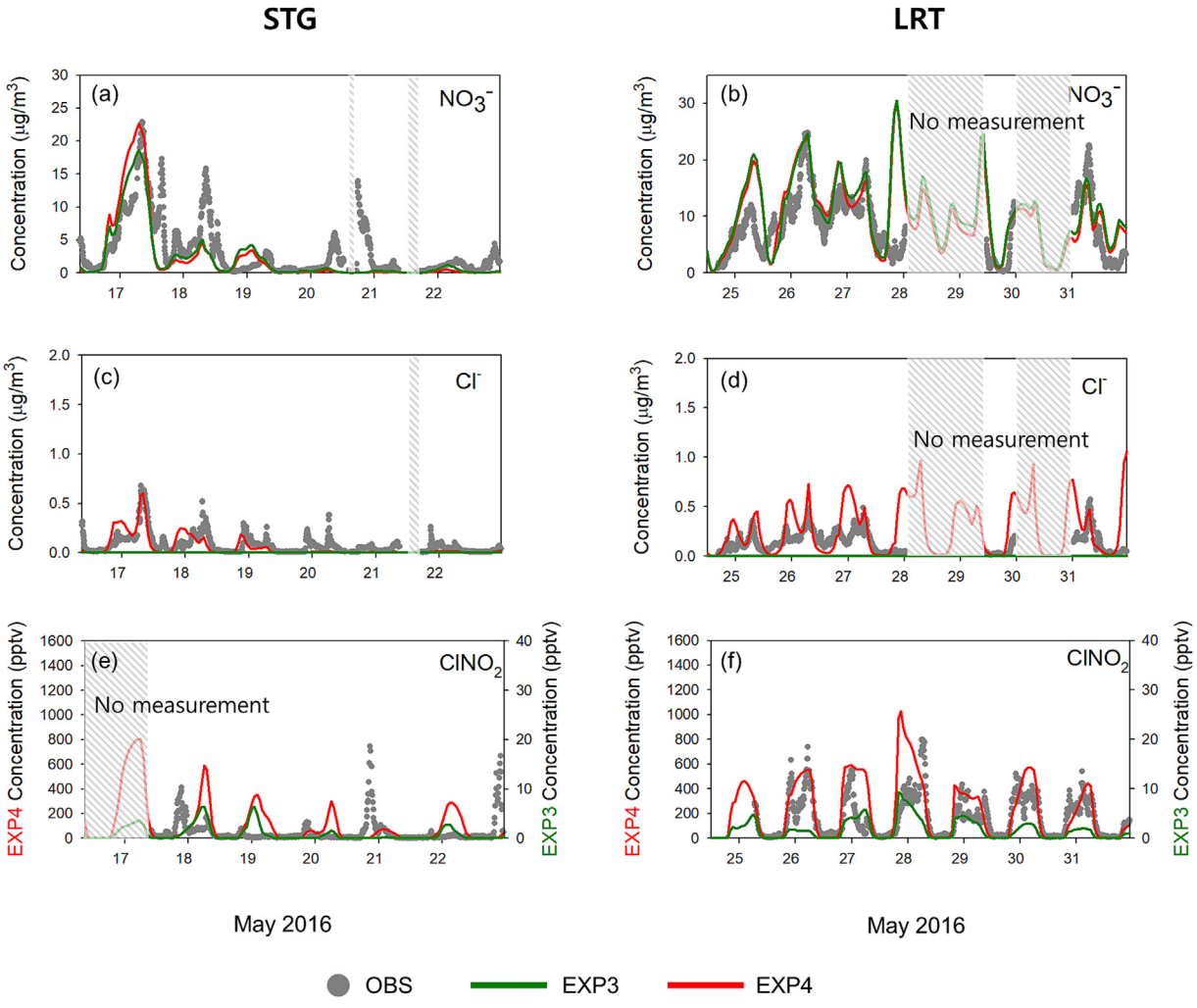

Fig. 8. Comparisons of time series measurements (at the OP site) for NO_3^-, Cl^-, and $ClNO_2$ against simulations from Exp3 and Exp4 for the stagnant (STG) and long-range transport (LRT) periods during the KORUS-AQ campaign. The gray shaded areas indicate missing time periods in the measurements.

sensitivity of formation of nitrate aerosol to the consideration of Cl-chemistry. The study found that the STG case had the highest NO_3^- HNO_3 concentration with a maximum hourly average of 23.6 μg m^{-3} (i.e., on May 17th), but the CMAQ sensitivity modeling by halving the N_2O_5 uptake coefficient showed the nitrate concentration decreased by around 27.1 % 74.5 % to 17.2 μg m^{-3}(see Fig. S3). The LRT case, on the other hand, showed a decrease of <10 %, indicating a small effect (Fig. S3). However, it is important to note that the study period was limited, and more extensive research would be needed.

4.4. Impact of anthropogenic Cl emissions over northeast Asia

To evaluate the contributions of Cl emissions (Fig. S1) to NO_3^- formation, Exp3 and Exp4 were compared in detail. The changes in hourly variation in their simulated NO_3^-, Cl^-, and $ClNO_2$ results against ground observations at the OP site are investigated. Fig. 8 shows that Exp4 also had some ability to simulate the higher NO_3^- concentrations and tended to be closer to the measurements than the other experiments. The daytime and night-time averages of NO_3^-, Cl^-, and $ClNO_2$ results against ground observations were also shown in Fig. S4. As with the Cl species in Fig. 8 and Fig. S4, however, it was confirmed that there was a clear difference in $ClNO_2$ and Cl^- between the two experiments, whereas there were no noticeable differences between inorganic species such as NO_3^- and NH_4^+ (<0.1 μg/m^3) as shown earlier in this study (Fig. S2) and in previous studies (Hong et al., 2020a, 2020b). One important observation related to the simulated Cl concentration is the noticeable inconsistency in Cl levels between the ground level and the non-surface atmosphere. Fig. 5 shows that Cl^- concentrations at ground level were generally consistent with observations, but model evaluations revealed a significant underestimation of Cl^- against non-surface aircraft measurements (Fig. 4). This implies that in urban areas with considerable surface anthropogenic Cl emissions, there would be significant fluctuations in the emissions of Cl species, and the uncertainties in Cl emissions need to be reduced. A more detailed model evaluation is needed over urban areas, particularly with regard to ground emissions sources.

In our analysis of the ground concentrations of Cl species, $ClNO_2$ began to accumulate at sunset and was rapidly photolyzed at sunrise, with a maximum measured concentration of approximately 800–1000 pptv (5 min average) during the nighttime (Fig. 8). The disregarding of both $ClNO_2$-chemistry and Cl emissions led to underestimations of the order of 1 ppb (or less) for $ClNO_2$ at the ground or near-surface level where many Cl emissions sources are located. In addition, by comparing $ClNO_2$ between Exp1 and Exp4, it was interpreted that the implementation of gas-phase $ClNO_2$ chemistry alone did not improve the prediction of $ClNO_2$. Further clarification of the role of Cl emissions in the $ClNO_2$ chemistry in the model is needed; for example, it increased the level of $ClNO_2$ significantly by a factor of more than two (i.e., May 28 in the LRT case) compared to Exp3 (Fig. 5). In addition, as indicated in previous studies, G/P partitioning is also an important process because it affects the NO_3^- production ratios in heterogeneous chemical reactions in many megacities over northeast Asia (e.g., Beijing, Shanghai, and Chongqing). In our study, it remained almost completely in the gas phase in the upper layer (i.e., at DC-8 aircraft

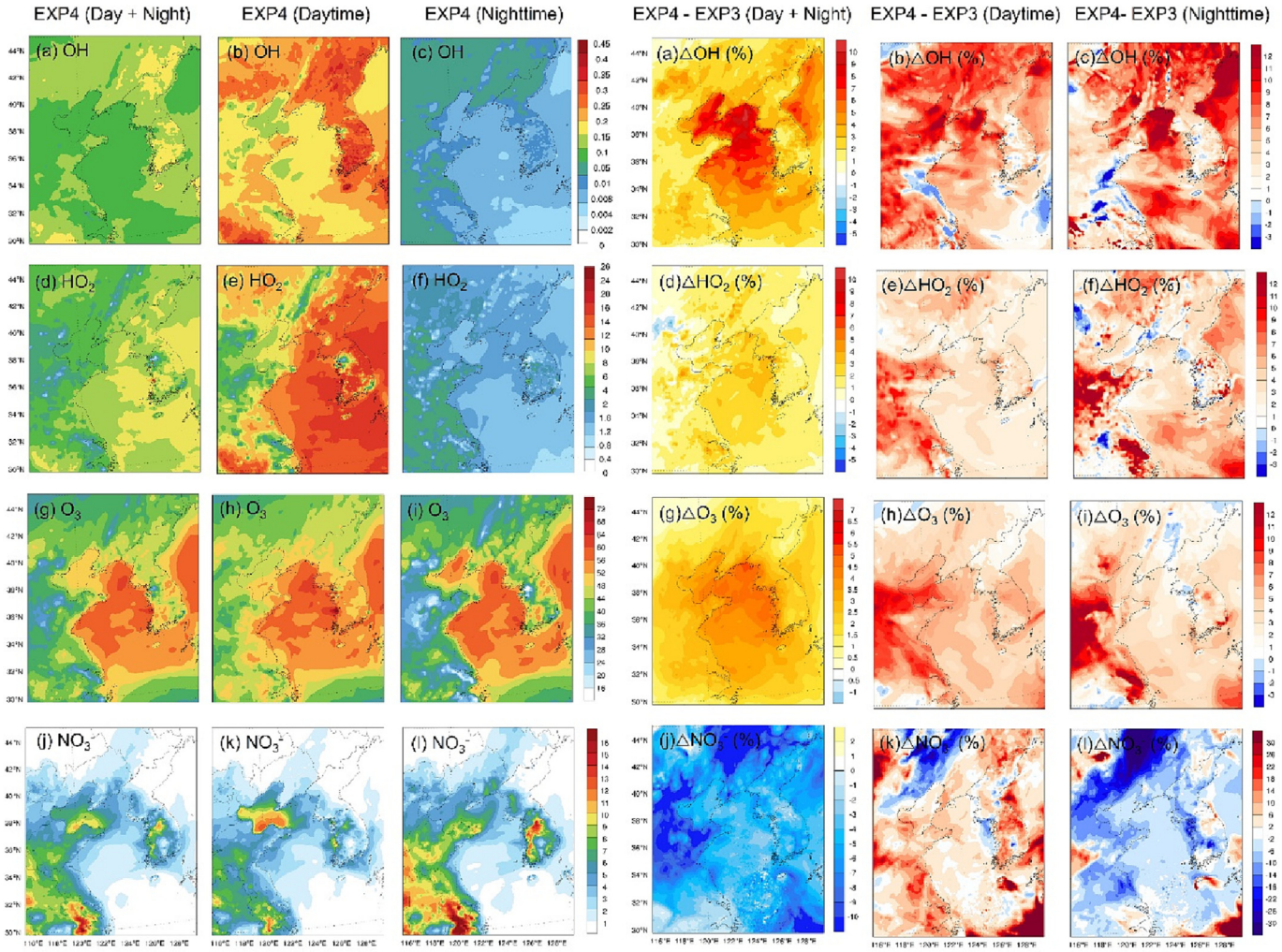

Fig. 9. Effect of anthropogenic chlorine emissions on several oxidants (OH, HO_2, O_3 and NO_3^-) in the surface air around South Korea over the entire KORUS-AQ campaign. All of the results were derived from Exp3 and Exp4, and the differences between the two experiments (Exp4 – Exp3).

measurement altitudes of 700–850 hPa) after G/P partitioning, resulting in decreased Cl^- concentrations (Fig. 4), which was not directly affected by emissions. Conversely, it was confirmed that the implementation of Cl emissions considerably decreased G/P partitioning, particularly in Exp4, contributing to the increase in Cl^- levels on the ground. This indicated that Cl emissions gave rise to more Cl^- that participated in the heterogeneous reaction and impacted the nighttime levels of nitrogen oxides (NO_2, NO_3, and N_2O_5). In Exp4, the results showed that the activation of both HCl and pCl^- emissions modulated the associated G/P partitioning through the $ClNO_2$ chemistry, resulting in increased Cl^- concentrations.

Previous studies have also shown that incorporating the $ClNO_2$ chemistry and Cl emissions has the potential to change the tropospheric oxidation capacity; Cl• can be produced through $ClNO_2$ photolysis, and can affect the surface O_3 levels in the morning (Li et al., 2016; Sarwar et al., 2012; Sarwar et al., 2014). In this study, we examined the spatiotemporal changes in major oxidants such as O_3 and HO_x species to interpret the changes in oxidation capacity through $ClNO_2$ chemistry and Cl emissions. This interpretation was also possible by comparing Exp4 with other experiments.

Fig. 9 shows the horizontal distributions of the differences in the major oxidants, i.e., O_3, OH, hydroperoxyl radical (HO_2), and NO_3 radicals between two experiments (Exp4 and Exp1). Differences were apparent for most species in high Cl emissions areas (Fig. S1), such as the areas in east China that were similarly described previously by Wang et al. (2022). In addition, changes were also observed over the downstream areas, particularly the marine areas around the Korean Peninsula (Fig. 9). Our numerical study indicated that OH and HO_2 concentrations increased on early morning, reducing the HNO_3 yield via (R6), and influencing the levels of both O_3 and daytime oxidants such as OH and HO_2, which were also impacted by the Cl• formed by the $ClNO_2$ photochemistry over northeast Asia. The oxidation capacity estimated from Exp4–Exp1 would drive changes in 1 h spatial averages of O_3 (+4.2 %: increase of 4.1×10^{10} molecules·cm^{-3}), OH (+7.2 %: increase of 1.27×10^5 molecules), and HO_2 (+10.0 %: increase of 2.2×10^6 molecules·cm^{-3}) concentrations over SMA in the early morning hours (0800–1000LST). However, Cl emissions (estimated from Exp4–Exp3) yielded small changes in O_3 (+0.5 %), OH (+1.1 %), and HO_2 (+1.8 %), respectively. The horizontal distributions of the changes in HO_x concentrations in Fig. 9 indicated small enhancements for all species (study domain average of <5 %). The increase in OH driven by Cl emissions and $ClNO_2$ chemistry led to a decrease in NO_x (see Fig. S5) because the principal sink of NO_x is through its oxidation by OH as mentioned in previous studies (Wang et al., 2020; Wang et al., 2022). Our simulations also indicated an increase in the NH_4^+ and Cl^- concentrations in and around the Korean Peninsula by up to 0.1 and 0.2 μg/m^3 (see Fig. S6), respectively, mainly because the emitted HCl under excess NH_3 caused NH_3 to transfer to NH_4^+, increasing the NH_4^+ and Cl^- concentrations via the reaction of HCl(g) + NH_3 (g) ↔ NH_4^+ + Cl^-. By contrast, NO_3^- concentrations were slightly decreased by up to 0.08 μg/m^3 due to the competition of N_2O_5 + Cl^- reactions with N_2O_5 hydrolysis, which is a major source of NO_3^-.

Fig. 10 shows spatiotemporal variation in changes in the NO_3^- and O_3 concentrations over the study area, arising from the effects of adding Cl emissions with $ClNO_2$ chemistry (Exp4–Exp1). The O_3 concentration increased during most hours (by a factor of ~5 %). Although it was not significant the largest changes occurred in the early hours of the morning (i.e., 0800–1000 LST) (Fig. 9), while NO_3^- decreased (~10 %) through both the day and night. From the temporal variation in O_3, NO_2, OH, and HO_2 (Figs. 4, 5, and S4), it could be interpreted that when the sun rises the following day and $ClNO_2$ is photo decomposed, NO_x is regenerated instead of HNO_3 being formed, which occurs during the nighttime. In the early daytime (i.e., 0800–1000 LST), Cl• preferentially increased the HO_x. This can be interpreted as an indication of the enhanced oxidative capacity activated by the $ClNO_2$ chemistry and Cl emissions during the early morning hours when HO_x generation is not completely activated.

In summary, adding $ClNO_2$ chemistry to the nighttime NO_3^- formation mechanism did not significantly alter the conclusions (particularly the levels of the inorganic species) of the base case where $ClNO_2$ chemistry and Cl emissions were not loaded. However, adding Cl emissions (such as

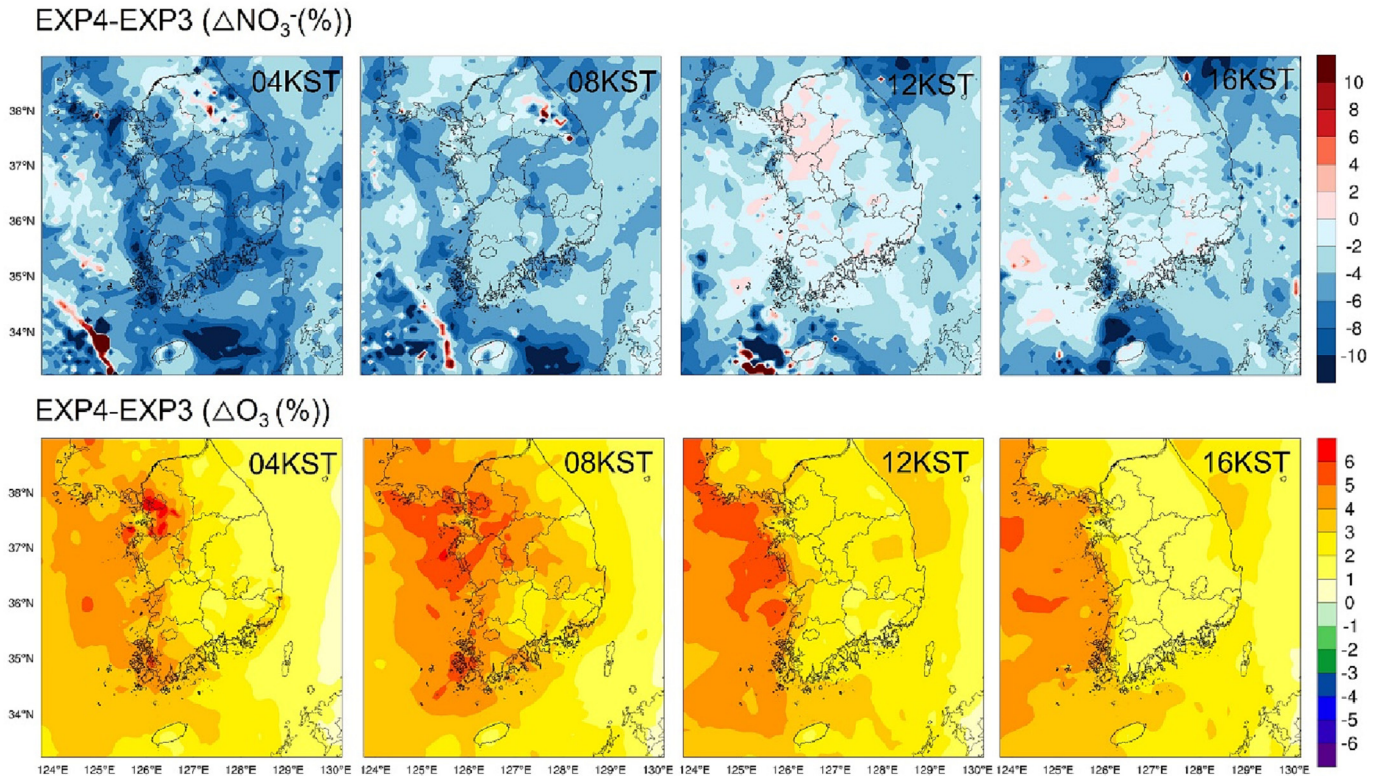

Fig. 10. Temporal variation in the differences in NO_3^- and O_3 in surface air around the Korean Peninsula with the inclusion of anthropogenic Cl emissions. All of the results were derived from Exp3 and Exp4, and the differences between the two experiments (Exp4 – Exp3).

pCl^- and HCl) produced the potential for better nighttime NO_3^- formation pathways. Subsequently, early morning O_3 and the oxidation capacity in the atmosphere over northeast Asia increased slightly (up to ~5 % of the domain average in this study) by activating Cl•, which also had a role in the intervention of other oxidation radicals such as HO_x. However, the uncertainties can still be further reduced, and the models should be evaluated in detail based on multiple measurements of Cl species.

In addition, more accurate emissions data are needed, including natural Cl emissions sources from other major source areas over northeast Asia. Natural Cl emissions can be estimated in the on-line model as a function of sea surface temperature and wind speed (Gong, 2015). Nevertheless, previous studies have indicated substantial uncertainties related to natural Cl emissions (Wang et al., 2020; Yang et al., 2022). Specifically, in the surf zone, where natural Cl emissions are highly influenced by zone width and whitecap coverage (Gantt et al., 2015), conducting emission verification studies is of utmost importance. Given this situation, it becomes crucial to achieve accurate estimation of natural Cl emissions as a prerequisite for their reliable application in regional modeling studies.

5. Summary and conclusions

We conducted a series of numerical sensitivity experiments to identify the role of $ClNO_2$ chemistry and Cl emissions on NO_3^- formation pathways by employing the WRF-CMAQ model and the latest HCl and pCl^- emissions over northeast Asia. The CMAQ with improved Cl heterogeneous chemistry and the latest HCl and Cl^- emissions were applied to northeast Asia during the 2016 KORUS-AQ campaign, and compared to extensive DC-aircraft and ground network observations for species related to heterogeneous Cl chemistry. Our WRF-CMAQ evaluation results showed that simulated Cl species against NASA DC-8 aircraft measurements indicated a significant underestimation in Cl^- simulations at higher altitudes (i.e., 700–850 hPa) but the $ClNO_2$ simulations were reasonable, suggesting that the thermodynamic module with the Cl-chemistry of Bertram and Thornton (2009) used in this study still requires improvement to achieve consistent Cl species simulations, particularly in the dry upper atmosphere . However, compared to surface (ground level) Cl species, the $ClNO_2$ and Cl- concentrations in urban areas showed a reasonable degree of consistency, but there were large fluctuations due to the uncertainties in ground-level Cl emissions.

The comparison of the results of the model sensitivity tests against measurements demonstrated that the N_2O_5 heterogeneous chemistry played an important role in the nighttime NO_3^- formation process. When the $ClNO_2$ chemical process was included in the N_2O_5 heterogeneous chemistry, the differences in the simulation results were minor, but the ability to simulate the $PM_{2.5}$ concentrations was slightly improved. For example, the NO_3^- and Cl^- results implied that a consideration of the $ClNO_2$ chemistry when considering the formation of N_2O_5 could improve the simulated concentrations of $PM_{2.5}$ and inorganic ions over the NOx-rich urban area.

When we considered anthropogenic Cl emissions, although the differences in NO_3^- and NH_4^+ were not significant (<0.1 mg/m^3), there was a clear difference in nighttime $ClNO_2$ and Cl^-. At sunrise on the following day, the generated nighttime $ClNO_2$ was photo decomposed, producing Cl• that affected the early morning O_3, OH, and HO_2 levels. We concluded that the effect of anthropogenic Cl emissions over the leeward marine area and Korean Peninsula decreased NO_3^- but increased the O_3, OH, and HO_2 levels, eventually leading to an increase in oxidation capacity over northeast Asia. Moreover, it is also important to consider the impacts of natural Cl emissions in association with nitrate. Thus, incorporating natural emissions into regional model studies is further necessary for a comprehensive understanding of the chlorine chemistry in Northeast Asia.

We also attempted to diagnose the oxidation capacities by considering Cl emissions, and the dominant contribution due to the increase in oxidation capacity was from OH at 66.6 % (max. increase of 1.21 × 10^6 molecules·cm^{-3}·s^{-1}), while O_3 and HO_2 accounted for 10.3 % and 0.3 %, respectively. The increase in total oxidation capacity was ~6.4 % in the early morning (0800–1000 LST) mainly due to the changes in OH (+7.2 %), HO_2 (+10.0 %), and O_3 (+4.2 %) across the Korean Peninsula, including the SMA in the early morning hours (0800–1000 LST) throughout the entire KORUS-AQ campaign period.

In conclusion, our findings improve understanding of NO_3^- formation and provide scientific information for the establishment of NO_3^- pollution control strategies over northeast Asia. More adequate quantitative measurements of Cl species are needed to diagnose the oxidation capacity except for the KORUS-AQ campaign period. Future studies need to include the development of an up-to-date anthropogenic (plus natural) Cl emissions inventory over northeast Asia to improve the quantification of N_2O_5 and $ClNO_2$ chemistry, the accuracy of NO_3^- simulations, and eventually determine their impact on air quality over northeast Asia.

CRediT authorship contribution statement

Hyun-young Jo: Conceptualization, Investigation, Visualization, Writing - original draft, Writing - Reviewing & Editing. **Jaehyeoung Park:** Software, Formal analysis. **Gookyoung Heo:** Writing - Reviewing & Editing. **Hyo-Jung Lee:** Investigation, Visualization. **Wonbae Jeon:** Software, Formal analysis. **Jong-Min Kim:** Investigation. **Saewung Kim:** Data curation. **Jung-Kwon Kim:** Cl emissions Verification, Data curation. **Yiming Liu:** Data curation. **Pengfei Liu:** Data curation. **Bingquing Zhang:** Data curation. **Cheol-Hee Kim:** Conceptualization, Investigation, Writing - Original draft, Writing - Reviewing & Editing, Supervision.

Data availability

No data was used for the research described in the article.

Declaration of competing interest

The authors declare that they have no known competing financial interests or personal relationships that could have appeared to influence the work reported in this paper.

Acknowledgements

This research was supported by the Basic Science Research Program through the National Research Foundation of Korea (NRF) funded by the Ministry of Education (2020R1A6A1A03044834 and 2020R1I1A1A01072998).

Appendix A. Supplementary data

Supplementary data to this article can be found online at https://doi.org/10.1016/j.scitotenv.2023.164920.

References

Appel, K.W., Napelenok, S.L., Foley, K.M., Pye, H.O.T., Hogrefe, C., Luecken, D.J., Bash, J.O., Roselle, S.J., Pleim, J.E., Foroutan, H., Hutzell, W.T., Pouliot, G.A., Sarwar, G., Fahey, K.M., Gantt, B., Gilliam, R.C., Heath, N.K., Kang, D., Mathur, R., Schwede, D.B., Spero, T.L., Wong, D.C., Young, J.O., 2017. Description and evaluation of the Community Multiscale Air Quality (CMAQ) modeling system version 5.1. Geosci. Model Dev. 10, 1703–1732.

Atkinson, R., 2000. Atmospheric chemistry of VOCs and NOx. Atmos. Environ. 34, 2063–2101.

Bertram, T.H., Thornton, J.A., 2009. Toward a general parameterization of N_2O_5 reactivity on aqueous particles: the competing effects of particle liquid water, nitrate and chloride. Atmos. Chem. Phys. 9, 8351–8363.

Chang, W.L., Brown, S.S., Stutz, J., Middlebrook, A.M., Bahreini, R., Wagner, N.L., Dubé, W.P., Pollack, I.B., Ryerson, T.B., Riemer, N., 2016. Evaluating N_2O_5 heterogeneous hydrolysis parameterizations for CalNex 2010. J. Geophys. Res. Atmos. 121, 5051–5070.

Crawford, J.H., Ahn, J.-Y., Al-Saadi, J., Chang, L., Emmons, L.K., Kim, J., Lee, G., Park, J.-H., Park, R.J., Woo, J.H., Song, C.-K., Hong, J.-H., Hong, Y.-D., Lefer, B.L., Lee, M., Lee, T., Kim, S., Min, K.-E., Yum, S.S., Shin, H.J., Kim, Y.-W., Choi, J.-S., Park, J.-S., Szykman, J.J., Long, R.W., Jordan, C.E., Simpson, L.J., Fried, A., Dibb, J.E., Cho, S., Kim, Y.P., 2021. The Korea-United States Air Quality (KORUS-AQ) field study. Elementa-Sci. Anthrop. 9 (1), 00163.

Emery, C., Liu, Z., Russell, A.G., Odman, M.T., Yarwood, G., Kumar, N., 2016. Recommendations on statistics and benchmarks to assess photochemical model performance. J. Air Waste Manage. Assoc. 67 (5), 582–598.

Finlayson-Pitts, B.J., Ezell, M.J., Pitts, J.N., 1989. Formation of chemically active chlorine compounds by reactions of atmospheric NaCl particles with gaseous N_2O_5 and $ClONO_2$. Nature 337, 241–244.

Gantt, B., Kelly, J.T., Bash, J.O., 2015. Updating sea spray aerosol emissions in the Community Multiscale Air Quality (CMAQ) model version 5.0.2. Geosci. Model Dev. 8, 3733–3746.

Gong, S.L., 2015. A parameterization of sea-salt aerosol source function for sub- and super-micron particles. Global Biogeochem. Cy. 17, 1097.

Guo, H., Sullivan, A.P., Campuzano-Jost, P., Schroder, J.C., Lopez-H, F.D., Dibb, J.E., Limenez, J.L., Thornton, J.A., Brown, S.S., Nenes, A., Webber, R.J., 2016. Fine particle pH and the partitioning of nitric acid during winter in the northeastern United States. J. Geophys. Res. Atmos. 121, 10,355–10,376.

Hong, Y., Liu, Y., Chen, X., Fan, Q., Chen, C., Chen, X., Wang, M., 2020a. The role of anthropogenic chlorine emission in surface ozone formation during different seasons over eastern China. Sci. Total Environ. 723, 137697.

Hong, Y., Liu, Y., Chen, X., Fan, Q., Chen, C., Chen, X., Wang, M., 2020b. The role of anthropogenic chlorine emission in surface ozone formation during different seasons over eastern China. Sci. Total Environ. 723, 137697.

Hurley, P.J., Blockley, A., Rayner, K., 2001. Verification of a prognostic meteorological and air pollution model for year-long predictions in the Kwinana industrial region of Western Australia. Atmos. Environ. 35 (10), 1871–1880.

Jeong, D., Seco, R., Gu, D., Lee, Y., Nault, B.A., Knote, C.J., Mcgee, T., Sullivan, J.T., Jimenez, J.L., Campuzano-Jost, P., Blake, D.R., Sanchez, D., Guenther, A.B., Tanner, D., Huey, L.G., Long, R., Anderson, B.E., Hall, S.R., Ullmann, K., Shin, H., Herndon, S.C., Lee, Y., Kim, D., Ahn, J., Kim, S., 2019. Integration of airborne and ground observations of nitryl chloride in the Seoul metropolitan area and the implications on regional oxidation capacity during KORUS-AQ 2016. Atmos. Chem. Phys. 19, 12779–12795.

Jo, H.-Y., Lee, H.-J., Jo, Y.-J., Lee, J.-J., Ban, J.-L., Chang, L.-S., Heo, G., Kim, C.-H., 2019. Nocturnal fine particulate nitrate formation by N_2O_5 heterogeneous chemistry in Seoul Metropolitan Area, Korea. Atmos. Res. 225, 58–69.

Jo, Y.-J., Lee, H.-J., Jo, H.-Y., Woo, J.-H., Kim, Y., Lee, T., Heo, G., Park, S.-M., Jung, D., Park, J., 2020. Changes in inorganic aerosol compositions over the Yellow Sea area from impact of Chinese emissions mitigation. Atmos. Res. 240, 104948.

Jo, H.-Y., Lee, H.-J., Jo, Y.-J., Heo, G., Lee, M., Kim, J.-A., Park, M.-S., Lee, T., Kim, S.-W., Lee, Y.-H., Kim, C.-H., 2022. A case study of heavy $PM_{2.5}$ secondary formation by N_2O_5 nocturnal chemistry in Seoul, Korea in January 2018: model performance and error analysis. Atmos. Res. 266, 105951.

Keene, C., Aslam, M., Khalil, K., Erickson, J., Archie, I.I.I., Graedel, E., Loberr, M., Aucott, M.L., Ling, S., Harper, D.B., Kleiman, G., Midgley, P., Moore, R.M., Seuzaret, C., Sturges, W.T., Benkovitz, C.M., Koropalov, V., Barrie, L.A., Li, Y.F., 1999. Composite global emissions of reactive chlorine from anthropogenic and natural sources: reactive chlorine emissions inventory. J. Geophys. Res. 104, 8429–8440.

Kim, C.-H., Park, S.-Y., Kim, Y.-J., Chang, L.-S., Song, S.-K., Moon, Y.-S., Song, C.-K., 2012. A numerical study on indicators of long-range transport potential for anthropogenic particulate matters over northeast Asia. Atmos. Environ. 58, 35–44.

Kim, C.-H., Lee, H.-J., Kang, J.-E., Jo, H.-Y., Park, S.-Y., Jo, Y.-J., Lee, J.-J., Yang, G.-H., 2018. Meteorological overview and signatures of long-range transport processes during the MAPS-Seoul 2015 campaign. Aerosol Air Qual. Res. 18, 2173–2184.

Kim, J.-M., Lee, H.-J., Jo, H.-Y., Jo, Y.-J., Kim, C.-H., 2021a. Vertical characteristics of secondary aerosols observed in the Seoul and Busan metropolitan areas of Korea during KORUS-AQ and associations with meteorological conditions. Atmosphere 12, 1451.

Kim, C.-H., Meng, F., Kajino, M., Lim, J., Tang, W., Lee, J.-J., Kiriyama, Y., Woo, J.-H., Sato, K., Kitada, T., Minoura, H., Kim, J., Lee, K.-B., Roh, S., Jo, H.-Y., Jo, Y.-J., 2021b. Comparative numerical study of $PM_{2.5}$ in exit-and-entrance areas associated with transboundary transport over China, Japan, and Korea. Atmosphere 12, 469.

Lee, H.-J., Jo, H.-Y., Park, S.-Y., Jo, Y.-J., Jeon, W., Ahn, J.-Y., Kim, C.-H., 2019. A case study of the transport/transformation of air pollutants over the Yellow Sea during the MAPS 2015 campaign. J. Geophys. Res. Atmos. 124, 6532–6553.

Lee, H.-J., Jo, H.-Y., Song, C.-K., Jo, Y.-J., Park, S.-Y., Kim, C.-H., 2020. Sensitivity of simulated $PM_{2.5}$ concentrations over Northeast Asia to different secondary organic aerosol modules during the KORUS-AQ campaign. Atmosphere 11, 1004.

Lee, H.-J., Chang, L.-S., Jaffe, D.A., Bak, J., Liu, X., Abad, G.G., Jo, H.-Y., Jo, Y.-J., Lee, J.-B., Kim, C.-H., 2021. Ozone continues to increase in East Asia despite decreasing NO_2: causes and abatements. Remote Sens. 13, 2177.

Lee, H.-J., Jo, Y.-J., Kim, S., Kim, D., Kim, J.-M., Choi, D., Jo, H.-Y., Bak, J., Park, S.-Y., Jeon, W., Kim, C.-H., 2022. Transboundary aerosol transport process and its impact on aerosol-radiation-cloud feedbacks in springtime over Northeast Asia. Sci. Rep. 12, 4870.

Li, Q., Zhang, L., Wang, T., Tham, Y.J., Ahmadov, R., Xue, L., Zhang, Q., Zheng, J., 2016. Impacts of heterogeneous uptake of dinitrogen pentoxide and chlorine activation on ozone and reactive nitrogen partitioning: improvement and application of the WRF-Chem model in southern China. Atmos. Chem. Phys. 16, 14875–14890.

Li, M., Zhang, Q., Kurokawa, J.I., Woo, J.H., He, K., Lu, Z., Ohara, T., Song, Y., Streets, D.G., Carmichael, G.R., Cheng, Y., Hong, C., Huo, H., Jiang, X., Kang, S., Liu, F., Su, H., Zheng, B., 2017. MIX: a mosaic Asian anthropogenic emission inventory under the international collaboration framework of the MICS-Asia and HTAP. Atmos. Chem. Phys. 17, 935–963.

Li, H., Zhang, Q., Zheng, B., Chen, C., Wu, N., Guo, H., Zhang, Y., Zheng, Y., Li, X., He, K., 2018. Nitrate-driven urban haze pollution during summertime over the North China Plain. Atmos. Chem. Phys. 18, 5293–5306.

Liu, Y.M., Fan, Q., Chen, X.Y., Zhao, J., Ling, Z.H., Hong, Y.Y., Li, W.B., Chen, X.L., Wang, M.J., Wei, X.L., 2018. Modeling the impact of chlorine emissions from coal combustion and prescribed waste incineration on tropospheric ozone formation in China. Atmos. Chem. Phys. 18, 2709–2724.

Monks, P.S., 2005. Gas-phase radical chemistry in the troposphere. Chem. Soc. Rev. 5, 34.

Osthoff, H.D., Roberts, J.M., Ravishankara, A.R., Williams, E.J., Lerner, B.M., Sommariva, R., Bates, T.S., Coffman, D., Quinn, P.K., Dibb, J.E., Stark, H., Burkholder, J.B., Talukdar, R.K., Meagher, J., Fehsenfeld, F.C., Brown, S.S., 2008. High levels of nitryl chloride in the polluted subtropical marine boundary layer. Nat. Geosci. 1, 324–328.

Park, I.-S., Choi, W.-J., Lee, T.-Y., Lee, S.-J., Han, J.-S., Kim, C.-H., 2005. Simulation of long-range transport of air pollutants over Northeast Asia using a comprehensive acid deposition model. Atmos. Environ. 39, 4075–4085.

Park, R.J., Oak, Y.J., Emmons, L.K., Kim, C.H., Pfister, G.G., Carmichael, G.R., Saide, P.E., Cho, S.Y., Kim, S., Woo, J.H., Crawford, J.H., Gaubert, B., Lee, H.-J., Park, S.-H., Jo, Y.-J., Gao, M., Tang, B., Stanier, C.O., Shin, S., Park, H., Bae, C., Kim, E., 2021. Multi-model intercomparisons of air quality simulations for the KORUS-AQ campaign. Elementa-Sci. Anthrop. 9, 00139.

Peterson, D., Hyer, E., Han, S.-O., Crawford, J., Park, R., Holz, R., Kuehn, R., Eloranta, E., Knote, C., Jordan, C., Lefer, B., 2019. Meteorology influencing springtime air quality, pollution transport, and visibility in Korea. Elementa-Sci. Anthrop. 7, 57.

Platt, U., LeBras, G., Poulet, G., Burrows, J.P., Moortgat, G., 1990. Peroxy radicals from night-time reaction of NO_3 with organic compounds. Nature 348, 147–149.

Sarwar, G., Simon, H., Bhave, P., Yarwood, G., 2012. Examining the impact of heterogeneous nitryl chloride production on air quality across the United States. Atmos. Chem. Phys. 12, 6455–6473.

Sarwar, G., Simon, H., Xing, J., Mathur, R., 2014. Importance of tropospheric $ClNO_2$ chemistry across the northern hemisphere. Geophys. Res. Lett. 41, 4050–4058.

Shon, Z.H., Kim, K.H., Song, S.K., Jung, K., Kim, N.J., Lee, J.B., 2012. Relationship between water-soluble ions in $PM_{2.5}$ and their precursor gases in Seoul megacity. Atmos. Environ. 59, 540–550.

Sommariva, R., Crilley, L.R., Ball, S.M., Cordell, R.L., Hollis, L.D.J., Bloss, W.J., Monks, P.S., 2021. Enhanced wintertime oxidation of VOCs via sustained radical sources in the urban atmosphere. Environ. Pollut. 274, 116563.

Souri, Amir H., Choi, Y., Jeon, W., Kochanski, A.K., Diao, L., Mandel, J., Bhave, P.V., Pan, S., 2017. Quantifying the impact of biomass burning emissions on major inorganic aerosols and their precursors in the U.S. J. Geophys. Res. Atmos. 122, 12,020–12,041.

Tian, M., Wang, H., Chen, Y., Zhang, L., Shi, G., Liu, Y., Yu, J., Zhai, C., Wang, J., Yang, F., 2017. Highly time-resolved characterization of water-soluble inorganic ions in $PM_{2.5}$ in a humid and acidic mega city in Sichuan Basin, China. Sci. Total Environ. 580, 224–234.

Tian, M., Liu, Y., Yang, F., Zhang, L., Peng, C., Chen, Y., Shi, G., Wang, H., Luo, B., Jiang, C., Li, B., Takeda, N., Koizumi, K., 2019. Increasing importance of nitrate formation for heavy aerosol pollution in two megacities in Sichuan Basin, southwest China. Environ. Pollut. 250, 898–905.

Wang, J.D., Zhao, B., Wang, S.X., Yang, F.M., Xing, J., Morawska, L., Ding, A.J., Kulmala, M., Kerminen, V.M., Kujansuu, J., Wang, Z.F., Ding, D.A., Zhang, X.Y., Wang, H.B., Tian, M., Petaja, T., Jiang, J.K., Hao, J.M., 2017. Particulate matter pollution over China and the effects of control policies. Sci. Total Environ. 584, 426–447.

Wang, X., Jacob, D.J., Eastham, S.D., Sulprizio, M.P., Zhu, L., Chen, Q., Alexander, B., Sherwen, T., Evans, M.J., Lee, B.H., Haskins, J.D., Lopez-Hilfiker, F.D., Thornton, J.A., Huey, G.L., Liao, H., 2019. The role of chlorine in global tropospheric chemistry. Atmos. Chem. Phys. 19, 3981–4003.

Wang, X., Jacob, D.J., Fu, X., Wang, T., Le Breton, M., Hallquist, M., Liu, Z., McDuffie, E.E., Liao, H., 2020. Effects of anthropogenic chlorine on $PM_{2.5}$ and ozone air quality in China. Environ. Sci. Technol. 54, 9908–9916.

Wang, H., Peng, C., Wang, X., Lou, S., Lu, K., Gan, G., Jia, X., Chen, X., Chen, J., Wang, H., Fan, S., Wang, X., Tang, M., 2022. N_2O_5 uptake onto saline mineral dust: a potential missing source of tropospheric $ClNO_2$ in inland China. Atmos. Chem. Phys. 22, 1845–1859.

Willmott, C.J., Ackleson, S.G., Davis, R.E., Feddema, J.J., Klink, K.M., Legates, D.R., O'Donnell, J., Rowe, C.M., 1985. Statistics for the evaluation and comparisons of models. J. Geophys. Res. 90 (C5), 8995–9005.

Xiao, H.-W., Zhu, R.-G., Pan, Y.-Y., Guo, W., Zheng, N.-J., Liu, Y.-H., Liu, C., Zhang, Z.-Y., Wu, J.-F., Kang, C.-A., Luo, L., Xiao, H.-Y., 2020. Differentiation between nitrate aerosol formation pathways in a southeast Chinese City by dual isotope and modeling studies. J. Geophys. Res. Atmos. 125 (13), e2020JD032604.

Yang, F., Tan, J., Zhao, Z., Du, Z., He, K., Ma, Y., Duan, F., Chen, G., Zhao, Q., 2011. Characteristics of $PM_{2.5}$ speciation in representative megacities and across China. Atmos. Chem. Phys. 11, 5207–5219.

Yang, T., Sun, Y., Zhang, W., Wang, Z., Liu, X., Fu, P., Wang, X., 2017. Evolutionary processes and sources of high-nitrate haze episodes over Beijing, Spring. J. Environ. Sci. 54, 142–151.

Yang, X., Wang, Q., Ma, N., Hu, W., Gao, Y., Huang, Z., Zheng, J., Yuan, B., Yang, N., Tao, J., Hong, J., Cheng, Y., Su, H., 2022. The impact of chlorine chemistry combined with heterogeneous N_2O_5 reactions on air quality in China. Atmos. Chem. Phys. 22 (3743–376).

Zhang, B., Shen, H., Yun, X., Zhong, Q., Henderson, B.H., Wang, X., Shi, L., Gunthe, S.S., Huey, L.G., Tao, S., Russell, A.G., Liu, P., 2022. Global emissions of hydrogen chloride and particulate chloride from continental sources. Environ. Sci. Technol. 56 (7), 3894–3904.